Wind Measurements on a Maneuvering Twin-Engine Turboprop Aircraft Accounting for Flow Distortion

ALASTAIR WILLIAMS AND DAVE MARCOTTE

Flight Research Laboratory, National Research Council, Ottawa, Ontario, Canada

(Manuscript received 10 August 1998, in final form 28 June 1999)

ABSTRACT

Traditional techniques for the calibration of the aircraft-relative wind vector from flight maneuvers are discussed with special regard to the effects of perturbations in the flow patterns around the aircraft body during periods of significant accelerations and angular rates (rapidly varying motion). A procedure is developed that allows both unbiased determination of steady-flight calibration parameters and explicit determination and characterization of errors in measured flow quantities that result from flow perturbations induced during the rapidly varying motion. This technique is applied to the case of air vector measurements from a five-hole pressure probe mounted under the wing of a Convair 580 research aircraft operated by the Canadian National Research Council. Results indicate that during pitching, yawing, and rolling maneuvers air data measurements at the pressure probe contain substantial errors that are associated with adjustments of the oncoming airflow to the sudden wing translations and rotations, as well as associated with variations in the strength and pattern of the along-wing sidewash circulation. In addition, the fuselage-measured static pressure position error is strongly affected by pressure pattern changes during strong longitudinal accelerations and, to a lesser extent, by lateral and normal accelerations during pitching and yawing motions. Empirical corrections to the pressure probe and static pressure measurements are derived to account for these effects, using multiple regression techniques. Under steady flight conditions, these corrections are small, but during rapid maneuvers they reduce the peak-to-trough errors in the derived earth-relative winds from ± 1.5 m s^{-1} (uncorrected) to around ± 0.6 m s^{-1} in the case of the horizontal wind components, and ± 0.4 m s^{-1} in the case of vertical wind components.

1. Introduction

Basic principles for determination of the three-dimensional wind vector from airborne platforms are well established (e.g., Lenschow 1986), and research groups worldwide are developing and operating wind measurement systems on aircraft (e.g., MacPherson 1990; Bögel and Baumann 1991; Lenschow et al. 1991; Tjernström and Friehe 1991; Crawford and Dobosy 1992; Whitmore et al. 1992). The enormous range in accuracy, complexity, and sophistication of individual installations is necessarily linked to performance and budgetary requirements, with systems designed for accurate high-resolution meteorological turbulence and flux measurements being among the most demanding. In recent years, this field has benefited from dramatic progress in aircraft position and motion sensing technology (e.g., Dobosy and Crawford 1996), sophisticated correction procedures for aircraft position and motion measurements (e.g., Shaw 1988; Leach and MacPherson 1991, 1994; Masters and Leise 1993), and new air motion sensing systems (e.g., Brown et al. 1983; Whitmore et al. 1992; Crawford and Dobosy 1992).

Although the calibration of airborne wind measurement systems is practically a ''science in itself,'' detailed critical discussions of such procedures appear only rarely in the literature (e.g., Bögel and Baumann 1991; Tjernström and Friehe 1991; Haering 1992). Central to this issue is the treatment of flow distortion effects (e.g., MacPherson and Baumgardner 1987; Cooper and Rogers 1991; MacPherson 1993; Crawford et al. 1996). Failure to compensate for the effects of flow distortion can lead to very significant errors in Reynolds stress and scalar flux measurements from aircraft (Wyngaard et al. 1985; Wyngaard 1991).

Many of the difficulties experienced in obtaining satisfactory and reliable results from wind calibrations may be attributable to the following interrelated characteristics of the measurement and calibration process.

- The wind vector cannot be measured directly but must be inferred via a complex nonlinear combination of more directly measurable components, all of which are subject to uncertainty in varying degrees.
- Many of the parameters required to ''connect'' these components are dependent upon properties of the dis-

Corresponding author address: Dr. Alastair Williams, Hadley Centre for Climate Prediction and Research, U.K. Meteorological Office, London Road, Bracknell, Berkshire RG12 2SY, United Kingdom.
E-mail: awilliams@meto.gov.uk

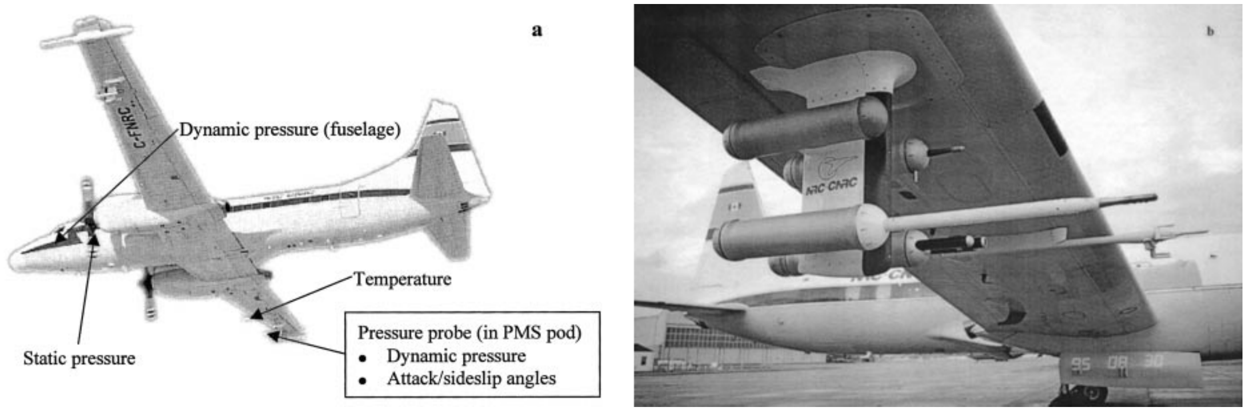

FIG. 1. NRC Convair 580, showing positions of air data sensors during this study. (a) Overview. (b) Close-up of wing, showing extended Rosemount-858AJ pressure probe mounted in lower outboard PMS canister (foreground), and showing Rosemount temperature probe mounted on underside of a separate boom farther inboard (background).

torted airflow in the direct vicinity of the measuring instruments during flight. Such parameters therefore are determinable only from carefully designed dedicated flight maneuvers and may lose their applicability outside a strict range of operating parameters or if the instrumentation is modified or relocated. (An obvious example is the upwash correction to angle of attack, which depends critically upon instrument location.)

- Flight maneuvers used for these purposes sometimes incorporate periods of rapidly varying motion, such as high-frequency pitches and yaws. Such maneuvers may not be appropriate for obtaining calibration parameters for use during steady flight, unless the calibration models consider possible variations in aircraft flow patterns during periods of significantly nonzero accelerations and angular rates.
- Commonly used calibration models and procedures are nonideal in their treatment of the interrelationships between essential components. They often require that raw (uncorrected) estimates of important quantities be used in the estimation of calibration parameters. Although such undesirable procedures are not completely avoidable (due to the highly nonlinear nature of the process), their use and effects can be minimized by careful design of the calibration analysis.

This paper details a calibration procedure that enables the calculation of winds of sufficient accuracy for use in boundary layer turbulence work from data obtained via measurement systems mounted on a Convair 580 (C580) twin-engine turboprop aircraft. The Flight Research Laboratory (FRL) of the Canadian National Research Council (NRC), which operates this aircraft primarily for cloud physics and aeromagnetics studies, has recently augmented its capabilities to include eddy correlation equipment for the measurement of fluxes of heat, moisture, momentum, and CO_2 in the atmospheric boundary layer, in a vein similar to that of the well-known Twin Otter aircraft, also operated by the FRL. Given that the NRC Convair mission flights usually have multiple objectives, it is often tempting to gather wind data during maneuvers that would normally be regarded as marginal in terms of data accuracy. Such maneuvers include spiraling ascents and descents, low-frequency ''porpoising'' (used to profile cloud layers), and steeply banked turns. Therefore, there is an interest to know which kinds of flight maneuvers can be executed without compromising the data accuracy significantly, as well as an interest to investigate the possibilities for data correction methods that may help to extend these boundaries.

As is often the case with multipurpose airborne research facilities, it is sometimes necessary to mount an instrument in a position that is not optimum. Such is the case with the C580 air motion measurement system, an extended Rosemount-858AJ pressure probe (for attack–sideslip angles, and static and dynamic pressure) mounted in one of four Particle Measuring Systems (PMS) canisters on a pod that is located 12.4 m, spanwise, along the wing, with its tip positioned only 0.52 m ahead of and 0.84 m below the leading edge of the wing (see Fig. 1). To minimize flow distortion effects, air-motion measurements are commonly made on booms ahead of the nose of an aircraft (as with the NRC Twin Otter), or from the holes in the nose of an aircraft (as in the radome system) (Brown et al. 1983; Tjernström and Friehe 1991). Such a configuration is not currently used by the C580, as the nose of the aircraft houses a ''spotlight'' synthetic aperture radar. As the analysis to follow will show, however, despite this nonideal configuration, it is possible to derive winds that remain accurate even during certain types of rapid maneuvers, provided that special attention is given to the variable effects of flow distortion in the calibration procedure. An important aspect of the current study is a method that allows explicit determination of the effects of flow perturbations induced during flight periods when accelerations and rotation rates are significantly nonzero. This greatly simplifies the process by which such effects can be characterized in terms of measured quantities.

TABLE 1. Measured air data quantities onboard the NRC Convair 580 aircraft. Superscripts/subscripts fus, pp, meas, and mir refer to "fuselage," "pressure probe," "measured," and "mirror," respectively.

Measured quantity	Description	Location	Type
$p^{\mathrm{fus}}_{\mathrm{meas}}$	Static pressure	Fuselage	DigiQuartz
$q^{\mathrm{fus}}_{\mathrm{meas}}$	Dynamic pressure	Fuselage	DigiQuartz
$\Delta P^{\mathrm{pp}}_{q}$	Differential pressure, dynamic (q)	Pressure probe	Rosemount-858AJ
$\Delta P^{\mathrm{pp}}_{\alpha}$	Differential pressure, attack angle (α)	Pressure probe	Rosemount-858AJ
$\Delta P^{\mathrm{pp}}_{\beta}$	Differential pressure, sideslip angle (β)	Pressure probe	Rosemount-858AJ
$T^{\mathrm{pp}}_{\mathrm{meas}}$	Total temperature	Near pressure probe	Rosemount 102DJ1CG
T_{mir}	Dewpoint (for humidity corrections)	Fuselage	EG&G cooled-mirror hygrometer

2. Wind measurements using the NRC Convair 580

The wind vector **U** in geodetic coordinates (x is east, y is north, z is up) may be calculated from aircraft measurements via the wind equation

$$\mathbf{U} = \tilde{\mathsf{M}}(\boldsymbol{\tau} + \boldsymbol{\Omega} \times \mathbf{r}) + \mathbf{G}, \tag{1}$$

where **G** is the aircraft ground-speed vector in geodetic coordinates, $\boldsymbol{\tau}$ is the relative wind ahead of the pressure probe, $\boldsymbol{\Omega}$ is the vector of angular "body" rates about the aircraft axes, and **r** is the (constant) position of the pressure probe. In (1), $\boldsymbol{\tau}$, $\boldsymbol{\Omega}$, and **r** are defined in aircraft-based coordinates (lon is longitudinal, lat is lateral, nrm is normal) and are converted to geodetic coordinates via the transformation matrix $\tilde{\mathsf{M}}$ (e.g., Lenschow 1972). The "lever arm" correction [$\tilde{\mathsf{M}}(\boldsymbol{\Omega} \times \mathbf{r})$] is formulated alternatively (e.g., Lenschow 1986) in terms of the time derivatives of the attitude angles, for which the relationship to the body rates is well known (e.g., Etkin 1963). (See appendix B for definition of variables.)

The aircraft-based coordinate system coincides with that of the LTN-91 Inertial Navigation System (INS), mounted at the Convair center of mass. The variable **G** is provided in real time directly by the INS, or it may be obtained in postflight reanalysis to an improved accuracy by combining high-frequency velocity components from the INS with low-frequency components from the NovAtel Global Positioning System (GPS), thereby eliminating low-frequency INS velocity errors (order of 1–2 m s^{-1}) associated with the Schuler Oscillation (Shaw 1988). The variable $\boldsymbol{\Omega}$ and the attitude angles (used in calculating $\tilde{\mathsf{M}}$) are also provided by the INS.

The relative wind vector $\boldsymbol{\tau}$ in aircraft coordinates is

$$\boldsymbol{\tau} = \begin{pmatrix} \tau_{\mathrm{lon}} \\ \tau_{\mathrm{lat}} \\ \tau_{\mathrm{nrm}} \end{pmatrix} = -\tau \begin{pmatrix} D^{-1} \\ D^{-1}\tan\beta \\ D^{-1}\tan\alpha \end{pmatrix}, \tag{2}$$

where α is the aircraft's angle of attack (positive if wind from below), β is the angle of sideslip (positive if wind from right), τ is true airspeed (magnitude of $\boldsymbol{\tau}$), and $D = (1 + \tan^2\alpha + \tan^2\beta)^{1/2}$. An approximate form of Eq. (2) is sometimes used by others (e.g., MacPherson 1990). The model used for the calculation of τ, α, and β onboard the Convair is based on the measured basic quantities in Table 1, for which accurate static calibrations are essential and known. The extended PMS canister-mounted 858 probe described in the introduction has been wind-tunnel tested at the NRC (MacPherson 1985) and has been flown on a variety of research aircraft, including the Convair (MacPherson 1993). For accurate wind computations, τ, α, and β must correspond to the *effective* (sometimes called "free stream") true airspeed and angles of attack and sideslip *in the undisturbed airstream ahead of the pressure probe.* The quantities measured at the probe will therefore need to be corrected for the effects of distortion in the flow near the wing of the aircraft.

Incorporated into the calibrations of the four basic pressure-related quantities (static and dynamic pressure, and the angles of attack and sideslip) are flow-distortion corrections for both steady and rapidly varying flight, the latter being denoted ε_x. For the purposes of this study, the term "rapidly varying" refers to periods in which aircraft accelerations and/or angular rates are significantly nonzero. The exact form of the corrections will be left undefined for the present. The major task of the subsequent sections is to assign empirical forms to these terms. We continue with the derivation of $\boldsymbol{\tau}$ using the corrected quantities.

Atmospheric static pressure at the altitude of the pressure probe p^{pp} is best estimated by correcting measurements made on the fuselage $p^{\mathrm{fus}}_{\mathrm{meas}}$ since probe-measured static pressure is overestimated significantly because of the proximity of the wing. Once the fuselage pressure has been corrected for flow effects, it is adjusted to the current height of the pressure probe to obtain p^{pp}. Free-stream dynamic pressure ahead of the pressure probe q^{pp} is estimated by correcting dynamic pressure measured at the probe $q^{\mathrm{pp}}_{\mathrm{meas}}$, which is the measured differential dynamic pressure $\Delta P^{\mathrm{pp}}_{q}$, adjusted for off-axis flow angles (see appendix A). In its extended configuration, the pressure probe reports local dynamic pressure to an accuracy of 0.4% or better for flow angles up to $\pm 15°$ (MacPherson 1985). If q^{pp} were to be estimated from $q^{\mathrm{fus}}_{\mathrm{meas}}$ (the fuselage-measured dynamic pressure), complex corrections would be required to account for attitude-related speed variations of the pressure pod relative to the fuselage. Such a method is possible but undesirable, as it would require a priori knowledge of τ and of the total temperature at the pod, which both depend on dynamic pressure (as discussed herein).

Once $p^{\rm pp}$ and $q^{\rm pp}$ are known, the following pressure-related quantity can be calculated, which defines the ratio of static to total temperatures in an adiabatic process:

$$p_{\gamma}^{\rm pp} = \left(\frac{p^{\rm pp}}{p^{\rm pp} + q^{\rm pp}}\right)^{(\gamma-1)/\gamma} = \frac{T^{\rm pp}}{\mathrm{TT}^{\rm pp}}. \qquad (3)$$

In the above equation, $T^{\rm pp}$ and $\mathrm{TT}^{\rm pp}$ are static and total temperatures in the vicinity of the pressure probe, and $\gamma = c_p/c_v$ is the ratio of specific heats for moist air at constant pressure and volume. Note that strictly speaking c_p and c_v (and therefore γ) are humidity dependent. In the Convair analysis, these quantities are computed as functions of the humidity mixing ratio (e.g., Riegel 1992, chapter X-C), which can be derived from water vapor partial pressure (a function of the dewpoint mirror temperature $T_{\rm mir}$) and $p^{\rm pp}$. Total temperature at the pressure probe can now be modeled as

$$\mathrm{TT}^{\rm pp} = \frac{\mathrm{TT}^{\rm pp}_{\rm meas}}{1 - (1 - r^{\rm pp})(1 - P^{\rm pp}_{\gamma})}, \qquad (4)$$

where $\mathrm{TT}^{\rm pp}_{\rm meas}$ is the measured total temperature and $r^{\rm pp}$ is the effective recovery factor of the temperature probe mounted near the pressure probe. Note that $r^{\rm pp}$ may have a slight Mach number dependency (Rosemount 1981). If the total temperature were measured far from the pressure probe, it would need to be corrected to the position of the pressure probe since total temperature depends upon local dynamic pressure. Once $\mathrm{TT}^{\rm pp}$ is known, static temperature (of the undisturbed airstream) at the pressure probe can be obtained from Eq. (3), and the true airspeed is then given by

$$\tau^{\rm pp} = [2c_p(\mathrm{TT}^{\rm pp} - T^{\rm pp})]^{1/2}. \qquad (5)$$

Note that the above equations for P_{γ}, TT, and τ can be derived easily from expressions in standard texts (e.g., Lenschow 1986).

The final step in calculating the relative wind vector is to obtain accurate estimates for the angles of attack and sideslip in the undisturbed flow ahead of the pressure probe $\alpha^{\rm pp}$ and $\beta^{\rm pp}$. This is achieved by correcting the local flow angles *at the probe* α_l and β_l, as calculated from the measured differential pressures $\Delta P^{\rm pp}_{\alpha}$, $\Delta P^{\rm pp}_{\beta}$, and $\Delta P^{\rm pp}_{q}$ using potential flow theory about a sphere. The exact formulas for the case of the Rosemount-858AJ pressure probe configuration upon the Convair are derived in appendix A. For small α, β, and an angle $\lambda = 45°$ between the central pressure port and any of the surrounding ports, the first-order estimates reduce to the following commonly used approximate expressions, after conversion from radians to degrees:

$$\alpha_1 \cong \frac{1}{f}\frac{\Delta P^{\rm pp}_{\alpha}}{\Delta P^{\rm pp}_{q}} \quad \text{and} \quad \beta_1 \cong \frac{1}{f}\frac{\Delta P^{\rm pp}_{\beta}}{\Delta P^{\rm pp}_{q}}, \qquad (6)$$

where $f = 0.0785\ \mathrm{deg}^{-1}$ is the α/β sensitivity factor. The wind tunnel tests of MacPherson (1985) confirm a close linear relationship between the ratio of the measured differential pressures and the flow angles with $f = 0.0780\ \mathrm{deg}^{-1}$, giving errors of 0.3° or better over a flow angle range of ±15°. The local flow angles α_l and β_l should be corrected for any alignment angle errors between the INS and the pressure probe axes, which were obtained from careful measurements on the ground, before finally treating the effects of flow distortion around the wing and mounting structures. Any residual alignment errors, as well as any effects of physical airframe distortions (such as wing flexing) during maneuvers, will also be aliased into these upwash–sidewash effects.

3. Estimation of calibration parameters from flight tests

a. Calibration philosophy

In designing a calibration procedure for airborne wind measurements within the restrictions of a given installation, the general objective is to identify suitable submodels for the various components, and then to calibrate and combine them in such a way that errors in the final calculated winds are minimized over the widest possible range of operating conditions. Clearly, the ideal calibration model is one in which all components are calibrated completely independently, and the resultant quantities are combined in exact equations to compute the wind vector. In such a model, residual errors can be tracked back directly to deficiencies in one or more of the individual calibration submodels. Such ideality is unreachable in practice (because of the complexity of airborne wind computations), and the best calibration procedure is one that minimizes the effects of component interrelationships (which lead to a need for intermediate approximations and an iterative evaluation of the parameter values between the submodels) and that maximizes the clarity with which residual errors can be related to deficiencies in specific contributing submodels.

In the current study, temperature and static pressure are calibrated independently using directly measured quantities. The steady part of the dynamic pressure and angle-of-attack calibrations are then obtained from measured quantities and from the corrected temperature and static pressure. The remaining quantities to be obtained are the sideslip-angle calibration for steady flight and any corrections to be applied to q, α, and β to account for the effects of rapidly varying motion. The analysis proceeds by recognizing that enough quantities are known accurately at this stage to invert the wind equation using a sensible guess for the ambient wind and to obtain the values of q, α, and β required to return that wind. These can now be used as reference quantities, first to calibrate the β during steady flight and then to

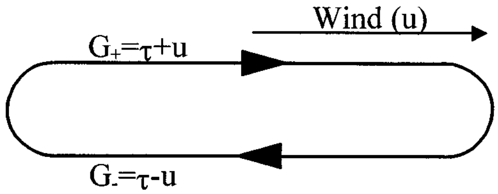

FIG. 2. Racetrack maneuver (see text for definition of symbols).

investigate the residual error in the computed q, α, and β resulting from flow perturbations during rapidly varying motion. In terms of the dataset used, this technique does not differ from an iterative calculation of parameters in the submodel equations for β and ε_x, based on a requirement to minimize the final wind error. (The input ''guess'' for the ambient wind in our technique is the same as the assumed ambient wind used as a benchmark for such a minimization.) However, the current method has the very significant advantage that since the errors in q, α, and β are explicitly calculated, the process of identifying flow-distortion problems, and then formulating and calibrating revisions to the submodels for each of these quantities, can be performed directly and independently.

b. Temperature

The derivation of the temperature recovery factor from test flight maneuvers is performed traditionally from gradual speed variations in straight-and-level flight, for which it can be shown that a plot of $\mathrm{TT}^{\mathrm{pp}}_{\mathrm{meas}}/T^{\mathrm{pp}}$ versus $M^2(\gamma - 1)/2$ [where $M = \tau/c_s$ is the Mach number, with the speed of sound $c_s = (\gamma R T^{\mathrm{pp}})^{1/2}$ and $R = c_p - c_v$] should yield a straight line with intercept 1 and slope r^{pp} (assuming constant T^{pp}). However, this requires a priori knowledge of both T^{pp} and τ, for which guesses must be made. For the Convair wind analysis, we prefer an approach suggested in a 1991 unpublished report by J. Leise and J. Masters, describing wind measurement on the National Oceanic and Atmospheric Administration (NOAA) P3 aircraft. In this method, racetrack maneuvers are flown directly into and with the wind at different airspeeds (see Fig. 2).

For any one racetrack flown at constant speed, the average of the squares of the ground speeds on the (straight and level) with-wind (G_+) and into-wind (G_-) legs is

$$G_{\mathrm{sqave}} = \frac{1}{2}(G_+^2 + G_-^2) = \frac{1}{2}[(\tau + u)^2 + (\tau - u)^2] = \tau^2 + u^2, \tag{7}$$

where u is wind speed (assumed constant). For racetracks at two different speeds,

$$\Delta G_{\mathrm{sqave}} = G_{\mathrm{sqave}}(\mathrm{fast}) - G_{\mathrm{sqave}}(\mathrm{slow}) = \tau^2(\mathrm{fast}) - \tau^2(\mathrm{slow}) = \Delta\tau^2. \tag{8}$$

Since it can be shown that $r^{\mathrm{pp}} = 2c_p\Delta\mathrm{TT}^{\mathrm{pp}}_{\mathrm{meas}}/\Delta\tau^2$, the temperature recovery factor can be derived using *only* the measured temperatures and ground speed (from INS/GPS), independent of any other measured or derived quantities. Note that $\mathrm{TT}^{\mathrm{pp}}_{\mathrm{meas}}$ should be corrected for aircraft height variations prior to this calculation, using an altitude measurement that is not pressure related (such as GPS or radar altitude if the flight is conducted over water).

In order for Eq. (8) to be valid, we note that the following three conditions must be satisfied for the two racetrack maneuvers, (i) wind speed and direction must be the same on all four legs, (ii) the four legs must be parallel and aligned with the assumed constant wind direction, and (iii) the true airspeed must be the same on the two legs of each racetrack. Although in practice a combination of precision piloting and careful choice of location and ambient meteorological conditions tends to keep the associated errors to an acceptable minimum, it is nevertheless important that racetrack maneuvers be repeated on independent occasions, in order to check the robustness of the derived effective recovery factor.

A value of $r^{\mathrm{pp}} = 0.94$ was obtained for the Rosemount temperature probe mounted near the pressure probe on the Convair. This is slightly smaller than the value of 0.975 quoted by Rosemount for this probe type [verified in wind tunnel tests of a similar probe by MacPherson (1978)], indicating that the local flow velocity at the probe position is slightly reduced relative to the overall aircraft airspeed. To a fair approximation, $r^{\mathrm{pp}}/r_T \cong \tau_L^2/\tau^2$ (MacPherson 1985), where r_T is the theoretical (or wind tunnel derived) recovery factor for the probe and τ_L is the local airspeed, from which we can estimate $\tau_L/\tau = 0.982$ for later reference.

c. Static pressure

As in other studies (e.g., Lenschow 1972; Tjernström and Friehe 1991), the ''position'' correction to fuselage-measured static pressure $p^{\mathrm{fus}}_{\mathrm{meas}}$ is modeled in terms of an offset error (C_0^p) and a steady-motion part based on the uncorrected fuselage-measured dynamic pressure $q^{\mathrm{fus}}_{\mathrm{meas}}$ accounting for speed dependence. In the current study, we employ a quadratic form for the $q^{\mathrm{fus}}_{\mathrm{meas}}$ dependence and then add a correction term for the effects of rapidly-varying motion (ε_p):

$$p^{\mathrm{fus}} = C_0^p + p^{\mathrm{fus}}_{\mathrm{meas}} + C^p_{q1}q^{\mathrm{fus}}_{\mathrm{meas}} + C^p_{q2}q^{\mathrm{fus}\ 2}_{\mathrm{meas}} + \varepsilon_p, \tag{9}$$

where p^{fus} is the corrected pressure, and C^p_{q1} and C^p_{q2} are quadratic regression coefficients. The rapidly varying part, which is expected to vanish during steady motion, is modeled as a linear combination of quadratics in the three orthogonal acceleration components (a_{lon}, a_{lat}, a_{nrm}):

$$\varepsilon_p = C^p_{\mathrm{lon1}}a_{\mathrm{lon}} + C^p_{\mathrm{lon2}}a^2_{\mathrm{lon}} + C^p_{\mathrm{lat1}}a_{\mathrm{lat}} + C^p_{\mathrm{lat2}}a^2_{\mathrm{lat}} + C^p_{\mathrm{nrm1}}a_{\mathrm{nrm}} + C^p_{\mathrm{nrm2}}a^2_{\mathrm{nrm}}. \tag{10}$$

Here, and in subsequent sections, symbols of the form

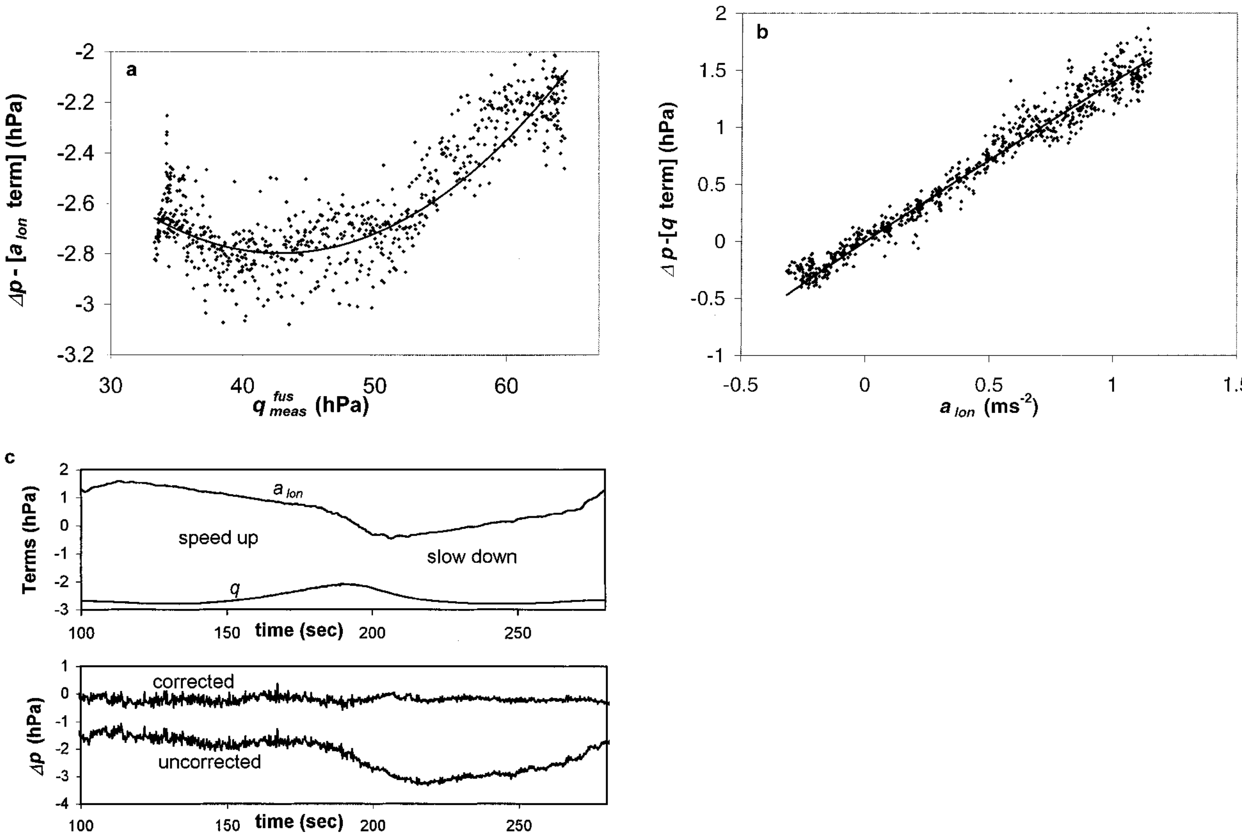

FIG. 3. Static pressure ''position'' error during a straight-and-level gradual acceleration–deceleration maneuver. (a) Dynamic pressure dependency and residuals. (b) Longitudinal acceleration dependency and residuals. (c) Contribution of various terms (upper panel) and final correction (lower panel): $\Delta p = \mathrm{mean}(p^{\mathrm{fus}}_{\mathrm{meas}}) - p^{\mathrm{fus}}_{\mathrm{meas}}$.

C^{v}_{wn} represent quadratic regression coefficients, with v and w denoting dependent and independent variables (respectively), and n indicating the degree of the coefficient.

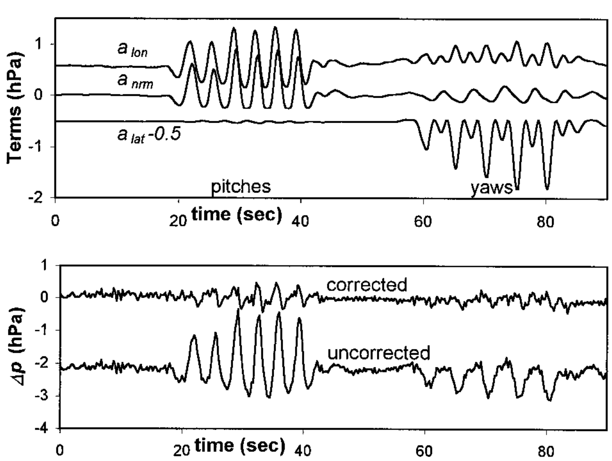

FIG. 4. Static-pressure rapidly varying corrections (ε_p) during pitch/yaw maneuvers. Upper panel: contribution of various terms. (For clarity, α_{lat} term is offset as indicated.) Lower panel: final correction. Here $\Delta p = \mathrm{mean}(p^{\mathrm{fus}}_{\mathrm{meas}}) - p^{\mathrm{fus}}_{\mathrm{meas}}$.

Quadratic forms are chosen in Eqs. (9) and (10), as some of the dependencies are expected to be nonlinear: for example, lateral and normal acceleration dependencies may be symmetric about zero. The form for ε_p is based upon the reasoning that during accelerated motion the pressure distribution about the fuselage of the aircraft will be perturbed relative to the steady-flight distribution. Note that the correction functions above are expected to be valid only over the range of airspeeds used during the flight maneuvers. In particular, application of Eq. (9) with the aircraft stationary on the ground (i.e., the case of $q^{\mathrm{fus}}_{\mathrm{meas}} = \varepsilon_x = 0$) is not valid, and we do not necessarily expect C^p_0 to be zero, as the pattern of airflow around the fuselage is fundamentally different.

The q and a_{lon} dependencies of static pressure (C^p_{q1}, C^p_{q2}, C^p_{lon1}, and C^p_{lon2}) are obtained first from a straight-and-level gradual acceleration–deceleration maneuver, using multiple regression analysis (Figs. 3a–c). Once the effects of q and a_{lon} are removed, the a_{nrm} and a_{lat} dependencies are subsequently established from rapidly varying pitch and yaw maneuvers, again using multiple regressions (Fig. 4). It should be noted that care is required when designing and performing multiple regression analyses upon data in which the regression quantities themselves can be correlated because spurious values for the derived coefficients may result. In the current analysis, it is useful that the a_{lon} dependency is derived from the acceleration–deceleration maneuver since in the pitching maneuver a_{lon} and a_{nrm} are correlated (Fig. 4). Prior to both analyses, measured static pressure has been adjusted to a constant altitude (the mean maneuver altitude) using an altitude measurement that is not pressure related. The pressure offset C_0^p is finally estimated by comparison of the (corrected) measured pressure with surface pressure during a low-level airfield ''missed approach'' (measured pressure at the lowest point having first been adjusted to ground level using radar altitude).

A quadratic component is apparent in the dynamic pressure correction term for static pressure ''position'' error on the Convair (Fig. 3a). Determinations of C_{q1}^p using a linear model in $q_{\mathrm{meas}}^{\mathrm{fus}}$ (e.g., Lenschow 1972) would thus produce results that vary depending upon the chosen speed range. A strong linear dependency upon the longitudinal component of acceleration is also apparent from the analysis (Fig. 3b), and the corrected terms for static pressure in the gradual acceleration–deceleration maneuver are shown in Fig. 3c. Furthermore, Fig. 4 shows that the effects of lateral and normal accelerations, although weaker, can also be significant. The derived set of static pressure correction parameters is given in Table 2.

We note that, strictly speaking, the q and a_{lon} dependencies should be investigated separately, in order to explore possible effects due to variations in the form of the q-dependency curve upon the value of a_{lon}. This could be accomplished for the case of $a_{\mathrm{lon}} = 0$ only by flying a series of straight-and-level runs at a range of constant speeds. Such a dataset was not available from the test flights used for this study, as the strong a_{lon} dependency was not foreseen.

For static pressure position error upon a Sabreliner aircraft, Tjernström and Friehe (1991) also reported a need to depart from a linear model in q, finding instead that a combination of 2 third-order polynomials (each valid over a different range of dynamic pressure) was required to cover the very large range of airspeeds treated in their study. Even after this rather complex correction, they found a residual hysteresis in their corrected pressures, which they attributed to varying flow regimes around the fuselage for accelerating and decelerating motion. It is clear that the flow around the Convair fuselage is similarly affected by accelerations. Tjernström and Friehe (1991) go on to suggest that such variations in flow regimes about the fuselage of their twin-engine jet may be explained by the change in role of the engines, which are acting more or less as air brakes when idling during decelerations. In the case of the Convair, it has been speculated that the large pressure drop across the propeller disks required to achieve a longitudinal acceleration could be the direct cause of the variations in the pressure distribution at the fuselage

TABLE 2. Derived model calibration parameters. Note that the stated parameters are valid for accelerations measured in meters per second squared, rates measured in degrees per second, and angles in degrees.

	Steady motion			Rapidly varying motion (ε_x)							
Temperature (°C)	r^{pp} 0.94										
Static pressure (hPa)	C_0^p 3.724	C_{q1}^p −0.1306	C_{q2}^p 0.001525	C_{lat1}^p −0.1943	C_{lat2}^p −0.2801	C_{lon1}^p 1.462	C_{lon2}^p −0.06347	C_{nrm1}^p −0.1768	C_{nrm2}^p 0.03101		
Dynamic pressure (hPa)		C_{q1}^q 0.989		$C_{\beta1}^q$ 0.2301	$C_{\beta2}^q$ −0.02404	C_{nrm1}^q −0.1815	C_{nrm2}^q −0.05494	C_{prt1}^q 0.07972	C_{prt2}^q −0.01150		
Attack angle (°)	C_0^α 0.4187	$C_{\alpha1}^\alpha$ 0.7058		$C_{\beta1}^\alpha$ −0.01736	$C_{\beta2}^\alpha$ 0.008618	C_{nrm1}^α 0.06703	C_{nrm2}^α −0.006896	C_{prt1}^α 0.09699	C_{prt2}^α −0.004365	C_{rrt1}^α 0.03352	C_{rrt2}^α −0.0003331
Sideslip angle (°)	C_0^β 2.139	$C_{\beta1}^\beta$ 0.9398		C_{lat1}^β −0.3854	C_{lat2}^β −0.1284	C_{nrm1}^β −0.08877	C_{nrm2}^β −0.03394	C_{prt1}^β 0.01749	C_{prt2}^β −0.01307		

static pressure port (only a few meters away), rather than the accelerations themselves. However, the data do not appear to support this hypothesis. For each of the two halves of the acceleration–deceleration maneuver, engine power was held at a near-constant value (this was confirmed postflight, as horsepower and propeller rotation rate were recorded variables), whereas the resultant a_{lon} varied much more gradually. As horsepower and a_{lon} were therefore not closely correlated, we would expect to see a marked hysteresis in the a_{lon}-dependency plot (Fig. 3b), the absence of which appears to indicate that the observed pressure distribution variations are more directly related to changes in a_{lon} itself rather than to engine power.

Bögel and Baumann (1991) also reported variations in static pressure position error during pitching and yawing maneuvers with the DLR Falcon aircraft, which Bögel and Baumann corrected empirically as functions of α and β. It is possible that these variations were equivalent to the errors corrected using normal and lateral acceleration components in the current study.

d. Dynamic pressure—Steady flight

The probe-measured dynamic pressure $q^{\text{pp}}_{\text{meas}}$ is corrected for flow distortion effects during steady motion via a multiplicative correction factor C^q_{q1} (e.g., Lenschow 1972), and a further possible correction ε_q is then added to account for the effects of rapidly varying motion, which will be dealt with in a later section:

$$q^{\text{pp}} = C^q_{q1} q^{\text{pp}}_{\text{meas}} + \varepsilon_q. \tag{11}$$

The coefficient C^q_{q1} is determined from the same along-wind-oriented racetrack maneuvers used for the temperature recovery factor analysis. Referring again to Fig. 2, for any one racetrack flown at constant airspeed, the average of the ground speeds of the with-wind and into-wind legs is τ:

$$G_{\text{ave}} = \frac{1}{2}(G_+ + G_-) = \frac{1}{2}[(\tau + u) + (\tau - u)] = \tau. \tag{12}$$

The error in *computed* true airspeed thus can be estimated as $G_{\text{ave}} - \tau$. The variable C^q_{q1} is deduced iteratively by comparing successive estimates of τ with G_{ave}, using Eqs. (3)–(5) with the corrected temperatures and static pressures determined above and assuming $\varepsilon_q = 0$ for steady flight. It should be noted that as in the procedure for the estimation of r^{pp} (section 3b), the relationship (12) is valid only under certain conditions. Figure 5 demonstrates the sensitivity of true airspeed error to the value of C^q_{q1} used for three racetrack patterns performed by the Convair at different airspeeds. The average zero-crossing C^q_{q1} for the three racetrack patterns is 0.989. Adoption of this constant value for C^q_{q1} implies uncertainties of less than ± 0.4 m s^{-1} in the derived true airspeed over the full Convair scientific operating airspeed range of 170–230 kt (88–119 m s^{-1})

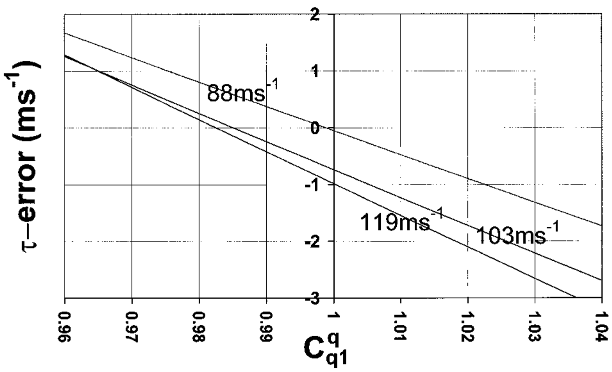

FIG. 5. True airspeed error as a function of the steady-flight dynamic pressure correction parameter C^q_{q1}, for three racetrack patterns at different speeds.

during steady flight. This value agrees well with the estimate obtained from the recovery factor analysis for the nearby temperature probe (section 3b). Wind tunnel tests of the extended PMS canister-mounted 858 probe by MacPherson (1985) have confirmed the theoretically expected value of 0.998 for the measured-to-free-stream velocity ratio (equivalent to τ_L/τ and closely related to C^q_{q1}), representing the effects of the canister-mounted probe geometry itself. The current results therefore indicate that the influence of the wing is to reduce q by only a additional 0.9% at the probe during steady flight. MacPherson and Baumgardner (1987) investigated the dependency of τ_L/τ upon the aircraft lift coefficient ($C_L = W/qA$, where W is aircraft gross weight and A is wing area) for the very same probe mounted in various positions under the wings of the NRC Twin Otter aircraft, and the National Center for Atmospheric Research (NCAR) Sabreliner and King Air aircraft. It was found that an appreciable C_L dependency was present only in the Twin Otter data, for which the probe was located in an area in which dynamic pressure (and therefore velocity) changes strongly with lift. The minimal variation of C^q_{q1} over the full sampling airspeed range in the current analysis indicates that the Convair installation does not place the probe in such a location.

e. Attack angle—Steady flight

The effective (free stream) aircraft angle of attack α^{pp} is obtained from the locally measured angle α_l by applying an offset (C^α_0) and sensitivity ($C^\alpha_{\alpha 1}$) correction to account for upwash effects during steady flight and by applying a possible further correction for the effects of rapidly varying motion (ε_α):

$$\alpha^{\text{pp}} = C^\alpha_0 + C^\alpha_{\alpha 1}\alpha_l + \varepsilon_\alpha. \tag{13}$$

The steady-flight upwash offset and sensitivity are obtained from straight-and-level gradual acceleration–deceleration maneuvers by comparison of α_l with the approximate reference attack angle α_{ref}, given by

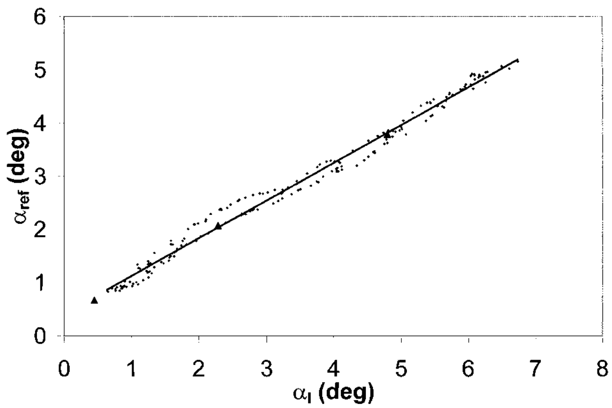

FIG. 6. Reference free-stream attack angle ($\alpha_{\rm ref}$) vs α at the pressure probe (α_l) for gradual acceleration–deceleration maneuver (dots) and racetracks (triangles). Here $C^{\alpha}_{\alpha 1}$ and C^{α}_{0} are given by the slope and the intercept of the best-fit line.

$$\sin(\alpha_{\rm ref}) = \tan\theta - \frac{G_z}{\tau\cos\theta}, \tag{14}$$

where θ is the aircraft pitch angle. This reference attack angle can be derived from Eq. (1) assuming that $U_z = \phi = \boldsymbol{\Omega} = \beta = 0$ (ϕ is aircraft roll angle) and $\cos\alpha \cong 1$ (for small α). To ensure that the varying longitudinal accelerations during the acceleration–deceleration maneuvers have not affected the value of $C^{\alpha}_{\alpha 1}$, the racetrack patterns are used to derive three additional points of comparison between α_l and $\alpha_{\rm ref}$. Results are displayed in Fig. 6, and the parameter values obtained are $C^{\alpha}_{\alpha 1} = 0.7058$ and $C^{\alpha}_{0} = 0.4187$.

The wind tunnel analysis of MacPherson (1985) has shown that the geometry of the extended canister-mounted probe alters the theoretical flow about the nose of the probe only very marginally. In particular, the α/β sensitivity factor f is reduced from 0.0785 to 0.0780. The value of $C^{\alpha}_{\alpha 1}$ derived above can therefore be attributed solely to an increase in upwash with lift, which is the expected behavior for airflow ahead of a wing. Note also that both $C^{\alpha}_{\alpha 1}$ and C^{α}_{0} may have a slight dependency upon Mach number, which is not investigated here (Tjernström and Friehe 1991; Haering 1992). The reader should refer to Crawford et al. (1996) for an interesting theoretical description of upwash effects, leading to predicted values for $C^{\alpha}_{\alpha 1}$ for a number of currently active research aircraft.

f. Reference quantities for sideslip angle and rapidly varying maneuvers

As introduced in section 3a, we now describe a general technique used for the derivation of reference values for dynamic pressure and attack/sideslip angles to be used in the determination of both the steady sideslip angle corrections and the remaining correction terms for rapidly varying motion. This technique requires an a priori estimate for the mean ambient wand vector $\mathbf{U}_{\rm est}$ during the period of the maneuver. A good method for providing this estimate in the absence of independent data is to compute ‘‘best-guess’’ winds using the aircraft data, with the corrected values of static and dynamic pressure and angle of attack derived above but assuming that $\beta^{\rm pp} = \beta_l$ and that the remaining rapidly varying correction terms are zero. The reference winds thus obtained will contain spurious variations resulting from the neglect of these terms, but their mean (or slowly varying) values provide an adequate guess for the ambient wind vector for current purposes.

The true airspeed vector $\boldsymbol{\tau}_{\rm rev}$ required to produce $\mathbf{U}_{\rm est}$ can be computed by inverting the wind equation, (1): $\boldsymbol{\tau}_{\rm rev} = \tilde{\mathbf{M}}^{-1}(\mathbf{U}_{\rm est} - \mathbf{G}) - \boldsymbol{\Omega} \times \mathbf{r}$. An iterative method is then used to find the values of true airspeed and attack/sideslip angles ($\tau_{\rm rev}$, $\alpha_{\rm rev}$, $\beta_{\rm rev}$) required to produce this true airspeed vector from Eq. (2):

1) $\alpha' = C^{\alpha}_{0} + C^{\alpha}_{\alpha 1}\alpha_l$ and $\beta' = \beta_l$ (first guesses for $\alpha_{\rm rev}$ and $\beta_{\rm rev}$)
2) $D' = (1 + \tan^2\alpha' + \tan^2\beta')^{1/2}$
3) $\tau_{\rm rev} = -\tau_{\rm lon}D'$, $\alpha_{\rm rev} = \tan^{-1}(-\tau_{\rm nrm}D'/\tau_{\rm rev})$, $\beta_{\rm rev} = \tan^{-1}(-\tau_{\rm lat}D'/\tau_{\rm rev})$ (Eq. 2)
4) $\alpha' = \alpha_{\rm rev}$, $\beta' = \beta_{\rm rev}$
5) Iterate back to step 2, until $\tau_{\rm rev}$, $\alpha_{\rm rev}$, and $\beta_{\rm rev}$ are constant to desired accuracy

Note that it is not theoretically necessary to use α_l and β_l in step 1 of the above loop ($\alpha' = \beta' = 0$ could have been used equally well as first guesses for $\alpha_{\rm rev}$ and $\beta_{\rm rev}$), as this calculation is fundamentally independent of the measured flow quantities. However, this practice speeds up the convergence process without affecting the values for $\tau_{\rm rev}$, $\alpha_{\rm rev}$, and $\beta_{\rm rev}$ that are obtained finally. Equipped with the desired value for $\tau_{\rm rev}$, we now compute

$$P_{\gamma,\rm rev} = \frac{X - r^{\rm pp}}{X + 1 - r^{\rm pp}},$$

where

$$X = \frac{\mathrm{TT}^{\rm pp}_{\rm meas}}{\mathrm{TT}^{\rm pp} - T^{\rm pp}} = \frac{2c_p}{\tau^2_{\rm rev}}\mathrm{TT}^{\rm pp}_{\rm meas},$$

which can be derived from Eqs. (4) and (5). Finally, from (3) we have

$$q_{\rm rev} = p^{\rm pp}(P^{\gamma/(1-\gamma)}_{\gamma,\rm rev} - 1).$$

The dynamic pressure and attack/sideslip angles $q_{\rm rev}$, $\alpha_{\rm rev}$, and $\beta_{\rm rev}$, computed as above, will be referred to as ‘‘reverse reference’’ quantities in the subsequent analysis.

g. Sideslip angle—Steady flight

In a fashion similar to the attack angle, the free-stream angle of sideslip $\beta^{\rm pp}$ is obtained from its local value β_l by applying an offset (C^{β}_{0}) and sensitivity ($C^{\beta}_{\beta 1}$) correction to account for sidewash effects during steady flight and by applying a possible further correction for rapidly varying motion (ε_β):

$$\beta_{\rm pp} = C_0^\beta + C_{\beta 1}^\beta \beta_l + \varepsilon_\beta. \tag{15}$$

In contrast to the attack angle, however, it is not as easy to modulate the sideslip angle in flight while maintaining the aircraft in steady motion. The sideslip sensitivity $C_{\beta 1}^\beta$ is derived commonly from high-frequency (rapidly varying) yawing motions by comparison with drift angle (track angle minus heading) or simply heading (Tjernström and Friehe 1991; Bögel and Baumann 1991). This practice makes use of the following simplified forms of the horizontal wind component equations, which can be obtained from Eq. (1) assuming small roll, pitch, and attack angles and by neglecting the lever arm correction:

$$U_x = G_x - \tau \sin(\varphi + \beta) \quad \text{and}$$

$$U_y = G_y - \tau \cos(\varphi + \beta) \tag{16}$$

where φ is the true heading. In these equations note that for constant wind and ground speed, small changes in φ are approximately balanced by changes in β (Tjernström and Friehe 1991), so that $\Delta\text{drift} = \Delta\beta$.

The use of Eqs. (16) is already a very crude approximation in the case of steady motion, and application to rapidly varying yawing maneuvers can lead to very scattered results. Tjernström and Friehe (1991) calibrated $C_{\beta 1}^\beta$ implicitly by iterative minimization of residual wind errors using the full wind equation, thereby avoiding the need to make this approximation, but were still unable to avoid the effects of rapidly varying motion. Our approach is to recognize that large variations in sideslip angle can be achieved while keeping accelerations and rotation rates to a minimum, if a "slow yawing" maneuver is performed in which a series of sideslip angles are produced and held while attempting to minimize roll. Drift angle is no longer a valid reference during such maneuvers since the aircraft track meanders significantly, but the reverse reference angle $\beta_{\rm rev}$ computed above can be used to estimate $C_{\beta 1}^\beta$ explicitly. Figure 7 presents a plot of $\beta_{\rm rev}$ versus β_l for a slow yawing maneuver, the slope of which returns $C_{\beta 1}^\beta$. The slight hysteresis reflects the fact that even during slow yaw maneuvers it is not possible to remove all rapidly varying effects with the Convair (in particular, a_{lat}; please see the next section).

The offset of the plot in Fig. 7 does not provide a good estimate for C_0^β since the mean value of $\beta_{\rm rev}$ is sensitive to offset errors in the chosen values for β when computing the reference wind. Luckily, a good estimate for C_0^β can be obtained by assuming $\varepsilon_\beta = 0$ during steady motion and then by applying Eq. (15) to reverse-heading runs within a racetrack pattern using drift angle as a reference:

$$C_0^\beta = 0.5\left[\overline{\text{drift}_+} + \overline{\text{drift}_-} - C_{\beta 1}^\beta(\overline{\beta_{l_+}} + \overline{\beta_{l_-}})\right], \tag{17}$$

where "+" and "−" denote with-wind and into-wind

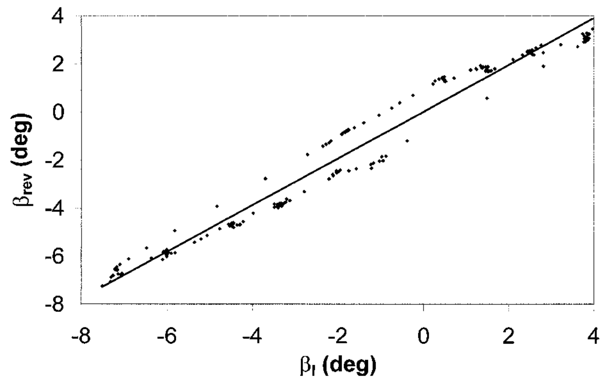

FIG. 7. Computed reverse-reference sideslip angle ($\beta_{\rm rev}$) vs sideslip angle at the pressure probe (β_l) for slow yawing maneuver. Here $C_{\beta 1}^\beta$ is given by the slope of the best-fit line.

legs of the racetrack, respectively, and an overbar denotes a leg-average quantity. The steady sideslip angle parameter values obtained for the Convair are $C_{\beta 1}^\beta = 0.9398$ and $C_0^\beta = 2.139$.

Under an aircraft wing, particularly near the wing tip, a sidewash (along wing) circulation occurs that may change with the angle of attack. The present results ($C_{\beta 1}^\beta$ close to 1) suggest that for the Convair installation this sidewash translates to a constant offset in β during steady motion. The three-aircraft study by MacPherson and Baumgardner (1987) reported a significant dependence of pod-measured β upon C_L only for the NCAR Sabreliner aircraft, which has a swept wing. In the present analysis, C_0^β and $C_{\beta 1}^\beta$ showed variations of only 0.12° and 7%, respectively, across the speed range of 88–119 m s^{-1}, indicating a negligible dependence of β upon both C_L and α.

The possibility that the flow angle offsets C_0^α and C_0^β may change with roll angle was also investigated as part of this study. However, it was found that during orbits with bank angles of up to 30°, C_0^α and C_0^β remained constant to within ±0.1°.

h. Corrections to q, α, and β for rapidly varying motion

Once values for C_0^β and $C_{\beta 1}^\beta$ have been derived, they are used to compute improved best-guess reference winds and, subsequently, new reverse reference quantities for use in the determination of the remaining rapidly varying correction terms. This analysis is performed using a sequence of pitch, yaw, and roll maneuvers. Figure 8 shows the computed winds uncorrected for rapidly varying motion, superimposed upon which is a least squares linear best fit used for the reference winds, removing all variability associated with the high-frequency motions. Below them are plotted differences between the values of q, α, and β required to obtain these winds (as computed by the process described in section 3f) and their values corrected for

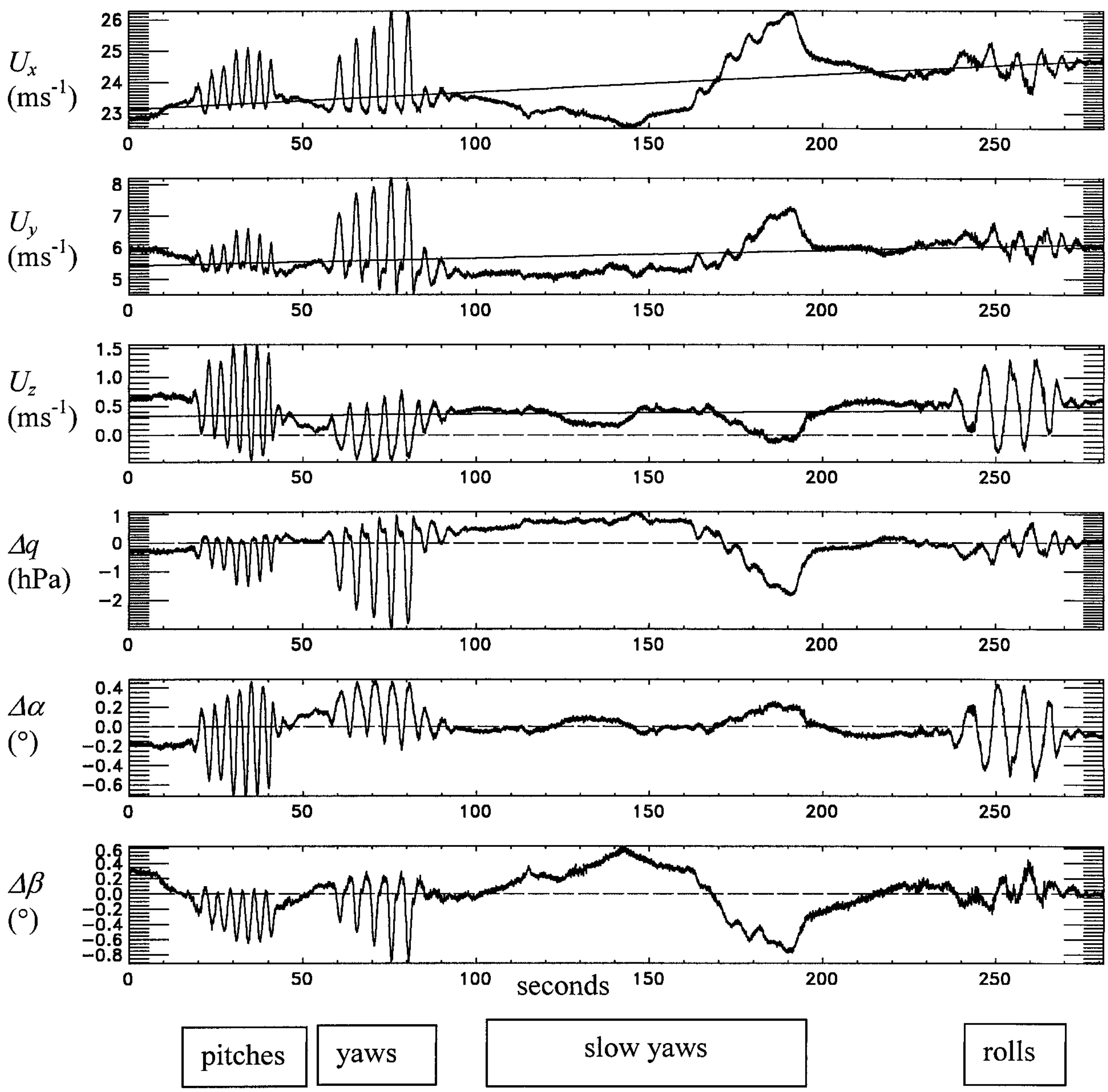

FIG. 8. Time series of computed quantities during pitch/yaw/roll maneuvers. Top three panels: wind components (m s^{-1}) uncorrected for rapidly varying motion, superimposed with linear regression lines used for the reference winds. Bottom three panels: Δq (hPa), $\Delta\alpha$, and $\Delta\beta$ (°) (''reverse''-reference minus steady-motion estimates).

steady-motion effects, as described above. These differences are denoted Δq, $\Delta\alpha$, and $\Delta\beta$ (Δ = ''reverse'' reference minus the steady-motion estimate). Clearly, errors associated with rapidly varying maneuvers can be as large as ± 1.5 hPa for q and $\pm 0.5°$ for α and β, producing wind errors from the Convair up to ± 1.5 m s^{-1}.

In addition to the three aircraft accelerations ($a_{\rm lon}$, $a_{\rm lat}$, $a_{\rm nrm}$) used in the analysis of the fuselage static pressure measurements, it was considered that an investigation of flow distortion effects in the vicinity of the pressure probe during rapidly varying motions should also include the three body rates ($\Omega_{\rm lon}$, $\Omega_{\rm lat}$, $\Omega_{\rm nrm}$) and the flow angles themselves (α, β). Nonzero angular rates can produce significant additional accelerations at the position of the probe (because of its location far from the aircraft's center of gravity) and, along with variations in the flow angles, can alter the form of flow over and along the wing. The differences Δq, $\Delta\alpha$, and $\Delta\beta$ were thus investigated relative to all of these quantities, once again using multiple regression analysis techniques.

A general regression was first performed upon each

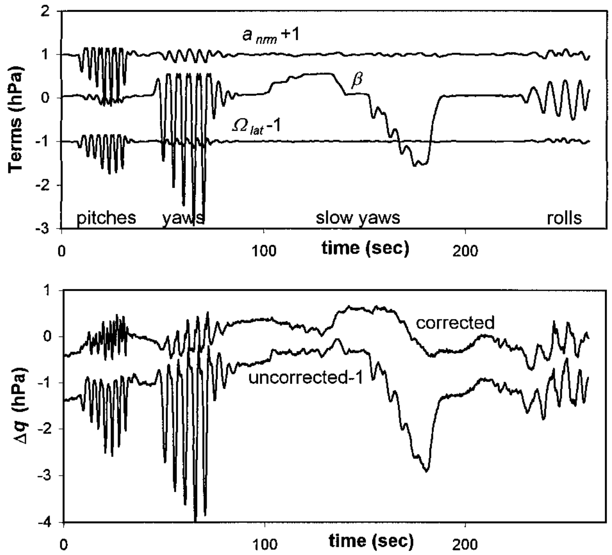

FIG. 9. Dynamic pressure rapidly varying corrections (ε_q) during pitch/yaw/roll maneuvers. Upper panel: contribution of various terms (for clarity, some are offset as indicated). Lower panel: final correction. Here $\Delta q = q_{\text{rev}} - q(\text{slow})$.

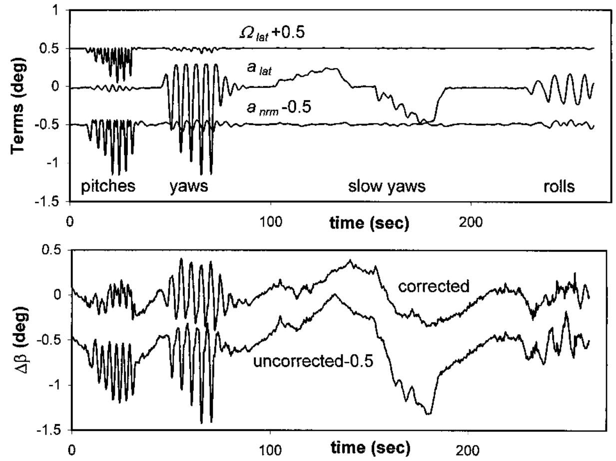

FIG. 10. Sideslip angle rapidly varying corrections (ε_β) during pitch/yaw/roll maneuvers. Upper panel: contribution of various terms. (For clarity, some are offset as indicated.) Lower panel: final correction. Here $\Delta\beta = \beta_{\text{rev}} - \beta(\text{slow})$.

Δ quantity versus linear and quadratic terms in all independent variables. Significant correlations discovered by this method were then explored in detail, using both the entire pitch/yaw/roll time series and individual maneuvers therein. In instances in which two (or more) independent variables were significantly correlated with a Δ quantity during a single maneuver, their intercorrelations were also investigated. If one variable could be discarded without significantly reducing the overall correlation with the Δ quantity, this was done. In such cases, the choice of variable to be retained was made on physical grounds, as far as possible. Finally, specific regressions were performed against the chosen subset of independent variables for each Δ quantity, and the following models for flow distortion corrections were established:

$$\varepsilon_\beta = C^\beta_{\text{lat1}} a_{\text{lat}} + C^\beta_{\text{lat2}} a^2_{\text{lat}} + C^\beta_{\text{nrm1}} a_{\text{nrm}} + C^\beta_{\text{nrm2}} a^2_{\text{nrm}} + C^\beta_{\text{prt1}} \Omega_{\text{lat}} + C^\beta_{\text{prt2}} \Omega^2_{\text{lat}} \tag{18}$$

$$\varepsilon_\alpha = C^\alpha_{\text{prt1}} \Omega_{\text{lat}} + C^\alpha_{\text{prt2}} \Omega^2_{\text{lat}} + C^\alpha_{\text{rrt1}} \Omega_{\text{lon}} + C^\alpha_{\text{rrt2}} \Omega^2_{\text{lon}} + C^\alpha_{\beta 1} \beta^{\text{pp}} + C^\alpha_{\beta 2} \beta^{\text{pp}^2} + C^\alpha_{\text{nrm1}} a_{\text{nrm}} + C^\alpha_{\text{nrm2}} a^2_{\text{nrm}} \tag{19}$$

$$\varepsilon_q = C^q_{\beta 1} \beta^{\text{pp}} + C^q_{\beta 2} \beta^{\text{pp}^2} + C^q_{\text{nrm1}} a_{\text{nrm}} + C^q_{\text{nrm2}} a^2_{\text{nrm}} + C^q_{\text{prt1}} \Omega_{\text{lat}} + C^q_{\text{prt2}} \Omega^2_{\text{lat}}, \tag{20}$$

where the subscripts ''prt'' and ''rrt'' denote coefficients associated with the pitch rate (Ω_{lat}) and the roll rate (Ω_{lon}), respectively. Note that the order of calculation is important, as corrections to q and α require the corrected β. The coefficients in the above formulations are presented in Table 2, and plots of the contributions to various error terms are presented in Figs. 9, 10 and 11.

Errors in all three air data quantities derived from the pressure probe are evident during pitching motions and can be reduced substantially via corrections based on pitch rate (Ω_{lat}) and normal acceleration (a_{nrm}). Note that Ω_{lat} and a_{nrm} are 90° out of phase during a pitching maneuver and therefore are uncorrelated, excluding the possibility of spurious correlations. Nonzero normal accelerations and pitch rates produce sudden vertical displacements and rotations (respectively) of the wing, which the oncoming airflow must adjust to over a finite time period. The effect upon q and attack angle can be explained as a delay in the adjustment of the oncoming flow vector to the movements of the wing, whereas variations in sideslip angle are likely to be attributable to adjustments in the pattern/strength of the along-wing (sidewash) circulation.

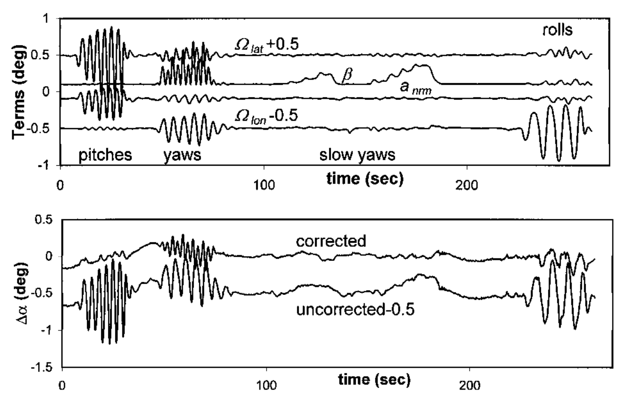

FIG. 11. Attack angle rapidly varying corrections (ε_α) during pitch/yaw/roll maneuvers. Upper panel: contribution of various terms. (For clarity, some are offset as indicated.) Lower panel: final correction. Here $\Delta\alpha = \alpha_{\text{rev}} - \alpha(\text{slow})$.

During yawing motions, both slow and fast, all three air data quantities again exhibited errors. In the case of $\Delta\beta$ (Fig. 10), these were corrected partially using lateral acceleration (a_{lat}). Although a dependence on a_{lat} seems understandable in terms of delayed adjustment of the oncoming flow to sideways wing movement while the aircraft is yawing, this correction is not entirely satisfactory as it overcorrects during fast yaws and undercorrects during slow yaws, leading to substantial residual errors (Fig. 10). A possible explanation is that distortion of the sidewash circulation pattern becomes more severe as the yawing frequency increases. Similar errors found in wind data from the NOAA P3 aircraft during high-frequency yawing maneuvers have also been attributed to variable time lags in air data quantities caused by such effects (J. Masters 1998, personal communication). In any case, the corrected sideslip angle (β) subsequently was used fairly successfully to correct errors in both Δq and $\Delta\alpha$ during yawing motions (Figs. 9 and 11).

During rolls, errors appear in Δq and $\Delta\beta$ (Figs. 9 and 10) that are corrected partially by the a_{lat} and β dependencies discussed above. In addition, however, $\Delta\alpha$ is correctable as a function of roll rate Ω_{lon} (Fig. 11), which is likely due to the additional vertical accelerations of the wing in the vicinity of the probe, induced by the roll rotation.

4. Discussion

In the absence of a sound physical description of flow around and along the Convair wing and fuselage during steady and rapidly varying motion, this study has been necessarily empirical in nature. Although attempts are occasionally made in the literature to derive relationships between aircraft motion parameters and airframe flow distortion fields on a more physical basis (Wyngaard et al. 1985; Crawford et al. 1996), the complexity and variability of such fields (both from aircraft to aircraft and as a function of location on any given aircraft) makes generalization of such relationships difficult. Although another approach is sophisticated numerical modeling of the flow about the wing, such studies still require empirical fitting of real flight data to model results.

In any case, it appears that our approach is effective. Figure 12 demonstrates the effects of the corrections derived above for rapidly varying motion upon the final computed wind vector. Errors associated with the violent pitch/yaw/roll maneuvers have been reduced substantially, with peak-to-trough values now being around ± 0.6 m s^{-1} for the horizontal components over a wide range of flying conditions (substantially less during steady flight). The vertical component of wind velocity U_z (critically important for meteorological turbulence and flux measurements) is in particularly good health, with errors during pitch maneuvers almost completely removed and errors during yaws and rolls reduced to around ± 0.4 m s^{-1} (peak to trough). In the horizontal wind components (U_x and U_y), the largest remaining errors appear during yawing maneuvers, probably attributable to complex adjustments in sidewash circulation patterns as β is varied, which remain uncompensated for. In addition to further flow distortion effects and possible influences of variations in flap settings, residual errors may be attributable at least partially to latencies and inaccuracies in the attitude and ground speed components obtained from the inertial navigation system (Bögel and Baumann 1991; Tjernstrom and Friehe 1991), which potentially could be removed in the future by Kalman filtering techniques (Leach and MacPherson 1991, 1994) or by the implementation of modern attitude differential GPS technology (Dobosy and Crawford 1996).

Acknowledgments. Alastair Williams wishes to recognize the extensive help and support provided by Dr. Ian MacPherson during Williams's time at the NRC Flight Research Laboratory in Ottawa. Thanks go to Jeffrey Masters, of the University of Michigan, for granting permission to use some concepts from his unpublished 1991 report that he prepared with James Leise. Patient technical assistance was provided by George Hoftyzer, Wilmer Budarick, and other members of the Convair crew. Piloting was performed by Captains John Aitken and John Croll. While in Canada, Dr. Williams was funded by the Natural Sciences and Engineering Research Council (NSERC) as a Visiting Fellow in a Canadian Government Laboratory.

APPENDIX A

Flow Angles and *q* at the Pressure Probe

The Rosemount-858 probe mounted in the FRL PMS canister (MacPherson 1985) consists of a conventional array of five pressure holes drilled into a hemispheric nose, with an additional static pressure measurement made via a ring of smaller holes drilled in a circle around the cylindrical housing, 3 in. back from the nose. The probe is plumbed/configured to supply the following outputs:

- $p^{\text{pp}}_{\text{meas}}$ Local static pressure,
- $\Delta P^{\text{pp}}_{\alpha}$ pressure difference between the lower and upper (attack) holes,
- $\Delta P^{\text{pp}}_{\beta}$ pressure difference between the right and left (sideslip) holes, and
- ΔP^{pp}_{q} pressure difference between the central hole and $p^{\text{pp}}_{\text{meas}}$

Elsewhere in this paper, static pressure at the probe altitude (p^{pp}) is derived using the fuselage static sensor $p^{\text{fus}}_{\text{meas}}$ since $p^{\text{pp}}_{\text{meas}}$ is elevated because of the proximity of the wing. However, $p^{\text{pp}}_{\text{meas}}$ remains the correct reference quantity for ΔP^{pp}_{q} since the central hole of the probe is also in the influence of the wing. It should also be noted

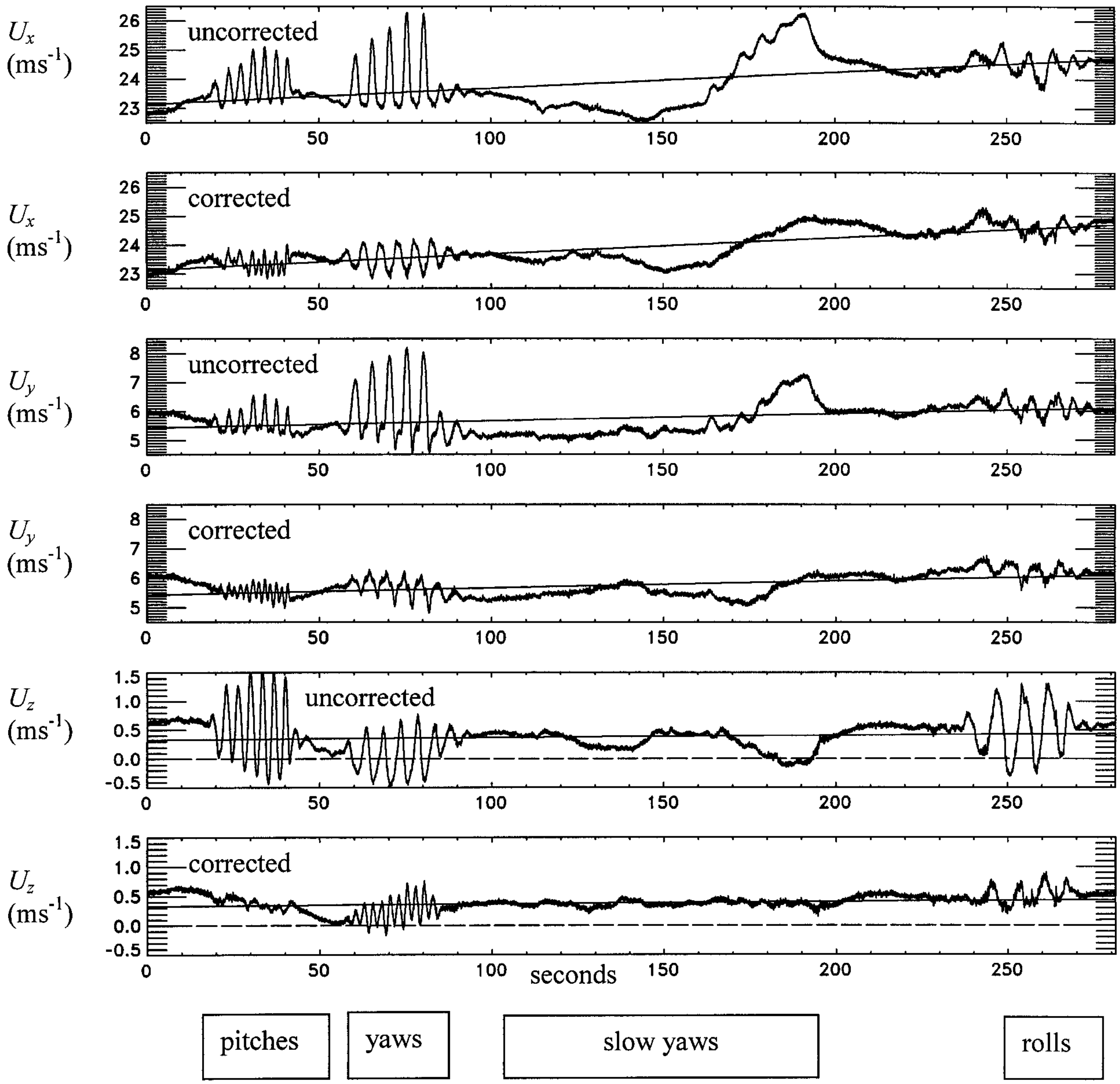

FIG. 12. Time series of computed quantities during pitch/yaw/roll maneuvers. Top two panels: east (x) wind component (m s^{-1}), uncorrected (upper) and corrected (lower) for rapidly varying motion; superimposed with linear regression line used for the ''reference'' wind. Middle two panels: north (y) wind component. Bottom two panels: vertical (z) wind component.

that ΔP_q^{pp} should not be equated with $q_{\mathrm{meas}}^{\mathrm{pp}}$, the local dynamic pressure at the probe, because there is a theoretical sensitivity of the central hole pressure measurement to flow angle. This is in contrast to the case of conventional pitot probes, which are relatively insensitive to flows at an angle to the longitudinal axis of the probe.

Part of the following derivation is drawn from the unpublished 1991 Leise and Masters report. We start with the well-known potential flow theory solution for the ideal pressure distribution over the surface of a sphere (e.g., Brown et al. 1983):

$$p(\zeta) = p_{\mathrm{meas}}^{\mathrm{pp}} + q_{\mathrm{meas}}^{\mathrm{pp}}\left(1 - \frac{9}{4}\sin^2\zeta\right),$$

where ζ is the angle between the (local) air vector and a surface port measuring pressure $p(\zeta)$. The cosine of this angle is found by forming the inner product between the unit vector $\hat{\mathbf{s}} = (s_{\mathrm{lon}}, s_{\mathrm{lat}}, s_{\mathrm{nrm}})$, pointing toward the pressure port from the center of the sphere, and the unit incident air vector $(1/D_l, \tan\beta_l/D_l, \tan\alpha_l/D_l)$, where α_l and β_l are the local flow angles at the probe and $D_l = (1 + \tan^2\alpha_l + \tan^2\beta_l)^{1/2}$. The quantity $\sin^2\zeta$ for use in the pressure distribution equation is thus given by

$$\sin^2\zeta = 1 - \cos^2\zeta$$
$$= 1 - \frac{(s_{\rm lon} + s_{\rm lat}\tan\beta_l + s_{\rm nrm}\tan\alpha_l)^2}{D_l^2}.$$

For the central hole, $\hat{\mathbf{s}} = (1, 0, 0)$, and we obtain

$$\Delta P_q^{\rm pp} = p_{\rm central} - p_{\rm meas}^{\rm pp} = q_{\rm meas}^{\rm pp}\left(\frac{9 - 5D_l^2}{4D_l^2}\right),$$

from which $q_{\rm meas}^{\rm pp}$ can be deduced for use in the wind analysis. Next, for an angle λ between the central and any other port on the pressure probe, the unit vectors pointing to the lower and upper attack angle ports are $\hat{\mathbf{s}} = (\cos\lambda, 0, \sin\lambda)$ and $\hat{\mathbf{s}} = (\cos\lambda, 0, -\sin\lambda)$, respectively, giving a differential pressure of

$$\Delta P_\alpha^{\rm pp} = (p_{\rm lower} - p_{\rm meas}^{\rm pp}) - (p_{\rm upper} - p_{\rm meas}^{\rm pp})$$
$$= -\frac{9}{4}q_{\rm meas}^{\rm pp}(\sin^2\zeta_{\rm lower} - \sin^2\zeta_{\rm upper})$$
$$= \frac{9}{2}\frac{q_{\rm meas}^{\rm pp}}{D_l^2}\tan\alpha_l\sin2\lambda.$$

After the same analysis for the sideslip angle, we arrive eventually at the following ratios:

$$\frac{\Delta P_\alpha^{\rm pp}}{\Delta P_q^{\rm pp}} = 18\frac{\tan\alpha_l\sin2\lambda}{9 - 5D_l^2} \quad \text{and}$$
$$\frac{\Delta P_\beta^{\rm pp}}{\Delta P_q^{\rm pp}} = 18\frac{\tan\beta_l\sin2\lambda}{9 - 5D_l^2}.$$

Defining the quantities

$$H_\alpha = \frac{2}{9\sin2\lambda}\frac{\Delta P_\alpha^{\rm pp}}{\Delta P_q^{\rm pp}} \quad \text{and} \quad H_\beta = \frac{2}{9\sin2\lambda}\frac{\Delta P_\beta^{\rm pp}}{\Delta P_q^{\rm pp}},$$

we see that

$$\left[1 - \frac{5}{4}(\tan^2\alpha_l + \tan^2\beta_l)\right]H_\alpha = \tan\alpha_l \quad \text{and}$$
$$\left[1 - \frac{5}{4}(\tan^2\alpha_l + \tan^2\beta_l)\right]H_\beta = \tan\beta_l.$$

For small angles, $\tan^2\alpha_l$ and $\tan^2\beta_l$ can be neglected, and also $\tan\alpha_l \simeq \alpha_l$ and $\tan\beta_l \simeq \beta_l$. The above equations thus reveal that H_α and H_β are first-order approximations for α_l and β_l. However, taking quotients gives $H_\alpha\tan\beta_l = H_\beta\tan\alpha_l$, from which decoupled quadratic equations can be formed and solved to yield exact solutions:

$$\tan\alpha_l = \frac{2H_\alpha}{1 + [1 + 5(H_\alpha^2 + H_\beta^2)]^{1/2}} \quad \text{and}$$
$$\tan\beta_l = \frac{2H_\beta}{1 + [1 + 5(H_\alpha^2 + H_\beta^2)]^{1/2}}.$$

APPENDIX B

Notation

a. Subscripts–superscripts

Geodetic coordinates: x is east, y is north, and z is up.
Aircraft coordinates: lon is longitudinal, lat is lateral, and nrm is normal.
Others: meas is measured, l is local, fus is fuselage, pp is pressure probe, ref–rev is reference–''reverse''-reference quantities (for calibration), $+/-$ is with-wind/into-wind, prt is pitch rate, and rrt is roll rate.

b. Parameters

Regression coefficients: C_{wn}^v, where v is the dependent variable, w is the independent variable, and n is the coefficient degree (0, 1, 2).

r	Effective recovery factor for temperature probe
C_L	Lift coefficient
f	α/β sensitivity factor
λ	Angle between central and any other port on pressure probe
$\mathbf{r}$	Vector position of pressure probe (aircraft coordinates)

c. Variables

$\mathbf{a}$	Aircraft acceleration vector (aircraft coordinates)
α, β	Effective aircraft angles of attack and sideslip
c_p, c_v	Specific heats for moist air at constant pressure and volume
D	Derived term containing airflow angles
ΔP_x	Differential pressures measured at the pressure probe ($x = q$, α, β)
ε_x	Correction terms for rapidly varying motion ($x = p$, q, α, β)
$\mathbf{G}$	Aircraft ground-speed vector (geodetic coordinates)
γ	Ratio of specific heats (c_p/c_v)
M	Mach number
$\tilde{\mathbf{M}}$	Transformation matrix, aircraft to geodetic coordinates
$\mathbf{\Omega}$	Vector of angular ''body'' rates about the aircraft axes (aircraft coordinates)
p	Static pressure
P_γ	Pressure term defining static-to-total temperature ratio in adiabatic process
q	Dynamic pressure
T	Static temperature
TT	Total temperature
$T_{\rm mir}$	Dewpoint mirror temperature
$\boldsymbol{\tau}$	Effective aircraft relative wind vector (aircraft coordinates)

τ True airspeed (magnitude of $\boldsymbol{\tau}$)
$\mathbf{U}$ Wind vector (geodetic coordinates)
u Wind speed (magnitude of $\mathbf{U}$)
θ, ϕ, φ Aircraft pitch, roll, and true heading angles
$\Delta\alpha, \Delta\beta, \Delta q$ Errors in α, β, q due to rapidly varying motion (Δ is the ''reverse''-reference quantity minus the steady-motion estimate).

REFERENCES

Bögel, W., and R. Baumann, 1991: Test and calibration of the DLR Falcon wind measuring system by maneuvers. *J. Atmos. Oceanic Technol.,* **8,** 5–18.

Brown, E. N., C. A. Friehe, and D. H. Lenschow, 1983: The use of pressure fluctuations on the nose of an aircraft for measuring air motion. *J. Climate Appl. Meteor.,* **22,** 171–180.

Cooper, W. A., and D. Rogers, 1991: Effects of airflow trajectories around aircraft on measurements of scalar fluxes. *J. Atmos. Oceanic Technol.,* **8,** 66–77.

Crawford, T. L., and R. J. Dobosy, 1992: A sensitive fast-response probe to measure turbulence and heat flux from any airplane. *Bound.-Layer Meteor.,* **59,** 257–278.

——, ——, and E. J. Dumas, 1996: Aircraft wind measurement considering lift-induced upwash. *Bound.-Layer Meteor.,* **80,** 79–94.

Dobosy, R. J., and T. L. Crawford, 1996: Accurate aircraft wind measurements using the global positioning system (GPS). *Proc. Conf. and Exhibition on Airborne Remote Sensing,* San Francisco, CA, ERIM International, 24–27.

Etkin, B., 1963: *Dynamics of Flight—Stability and Control.* Wiley and Sons, 519 pp.

Haering, E. A., Jr., 1992: Airdata calibration techniques for measuring atmospheric wind profiles. *J. Aircraft,* **29,** 632–639.

Leach, B. W., and J. I. MacPherson, 1991: An application of Kalman filtering to airborne wind measurement. *J. Atmos. Oceanic Technol.,* **8,** 51–65.

——, and ——, 1994: Comments on ''Correction of inertial navigation with Loran C on NOAA's P-3 aircraft.'' *J. Atmos. Oceanic Technol.,* **11,** 1048–1053.

Lenschow, D. H., 1972: The measurement of air velocity and temperature using the NCAR Buffalo aircraft measuring system. NCAR Tech. Note EDD-74, 39 pp. [Available from UCAR Communications, P.O. Box 3000, Boulder, CO 80307-3000.]

——, 1986: Aircraft measurements in the boundary layer. *Probing the Atmospheric Boundary Layer,* D. H. Lenschow, Ed., Amer. Meteor. Soc., 39–55.

——, E. R. Miller, and R. B. Friesen, 1991: A three-aircraft intercomparison of two types of air motion measurement systems. *J. Atmos. Oceanic Technol.,* **8,** 41–50.

MacPherson, J. I., 1978: Wind tunnel and flight tests of temperature probes used on the NAE T-33 and Twin Otter atmospheric research aircraft. NRC Report NAE LTR-FR-62, 34 pp. [Available from Flight Research Laboratory, National Research Council, Ottawa, ON K1A 0R6, Canada.]

——, 1985: Wind tunnel calibration of a PMS canister instrumented for airflow measurement. NRC Report NAE NAE-AN-32, 63 pp. [Available from Flight Research Laboratory, National Research Council, Ottawa, ON K1A 0R6, Canada.]

——, 1990: Wind and flux calculations on the NAE Twin Otter. NRC Report NAE LTR-FR-109, 38 pp. [Available from Flight Research Laboratory, National Research Council, Ottawa, ON K1A 0R6, Canada.]

——, 1993: Use of a wing-mounted airflow pod for airborne wind and flux measurement. Preprints, *Eighth Symp. on Meteorological Observations and Instrumentation,* Anaheim, CA, Amer. Meteor. Soc., 169–174.

——, and D. Baumgardner, 1987: Studies of aircraft flow effects about wing-mounted PMS probes. Preprints, *Sixth Symp. on Meteorological Observations and Instrumentation,* New Orleans, LA, Amer. Meteor. Soc., 144–147.

Masters, J. M., and J. A. Leise, 1993: Correction of inertial navigation with Loran C on NOAA's P-3 aircraft. *J. Atmos. Oceanic Technol.,* **10,** 145–154.

Riegel, C. A., 1992: *Fundamentals of Atmospheric Dynamics and Thermodynamics,* World Scientific, 496 pp.

Rosemount, 1981: Total temperature sensors. Rosemount Engineering Company Technical Bulletin 5755 (Rev. A), 29 pp. [Available from Rosemount Engineering Company, P.O. Box 35129, Minneapolis, MN 55435.]

Shaw, W. J., 1988: Inertial drift correction for aircraft-derived wind fields. *J. Atmos. Oceanic Technol.,* **5,** 774–782.

Tjernström, M., and C. A. Friehe, 1991: Analysis of a radome air-motion system on a twin-jet aircraft for boundary-layer research. *J. Atmos. Oceanic Technol.,* **8,** 19–40.

Whitmore, S. A., T. R. Moes, and T. J. Larson, 1992: High angle-of-attack flush air data sensing system. *J. Aircraft,* **29,** 915–919.

Wyngaard, J. C., 1991: On the maintenance and measurement of scalar fluxes. *Land Surface Evaporation—Measurement and Parameterization,* T. J. Schmugge, and J.-C. André, Eds., Springer-Verlag, 199–229.

——, L. Rockwell, and C. A. Friehe, 1985: Errors in the measurement of turbulence upstream of an axisymmetric body. *J. Atmos. Oceanic Technol.,* **2,** 605–614.